Journal of Biomechanics 59 (2017) 35–42

Contents lists available at ScienceDirect

Journal of Biomechanics

journal homepage: www.elsevier.com/locate/jbiomech
www.JBiomech.com

Microfluidic co-culture platform for investigating osteocyte-osteoclast signalling during fluid shear stress mechanostimulation

K. Middleton [a], S. Al-Dujaili [a], X. Mei [b], A. Günther [a,b], L. You [a,b,*]

[a] Institute of Biomaterials and Biomedical Engineering, University of Toronto, 164 College Street, Toronto, Ontario M5S 3G9, Canada
[b] Department of Mechanical and Industrial Engineering, University of Toronto, 5 King's College Road, Toronto, Ontario M5S 3G8, Canada

ARTICLE INFO

Article history:
Accepted 13 May 2017

Keywords:
Mechanobiology
Fluid flow shear stress
Microfluidic
Osteocytes
Osteoclasts
Co-culture

ABSTRACT

Bone cells exist in a complex environment where they are constantly exposed to numerous dynamic biochemical and mechanical stimuli. These stimuli regulate bone cells that are involved in various bone disorders, such as osteoporosis. Knowledge of how these stimuli affect bone cells have been utilised to develop various treatments, such as pharmaceuticals, hormone therapy, and exercise. To investigate the role that bone loading has on these disorders *in vitro*, bone cell mechanotransduction studies are typically performed using parallel plate flow chambers (PPFC). However, these chambers do not allow for dynamic cellular interactions among different cell populations to be investigated. We present a microfluidic approach that exposes different cell populations, which are located at physiologically relevant distances within adjacent channels, to different levels of fluid shear stress, and promotes cell-cell communication between the different channels. We employed this microfluidic system to assess mechanically regulated osteocyte-osteoclast communication. Osteoclast precursors (RAW264.7 cells) responded to cytokine gradients (e.g., RANKL, OPG, PGE-2) developed by both mechanically stimulated (fOCY) and unstimulated (nOCY) osteocyte-like MLO-Y4 cells simultaneously. Specifically, we observed increased osteoclast precursor cell densities and osteoclast differentiation towards nOCY. We also used this system to show an increased mechanoresponse of osteocytes when in co-culture with osteoclasts. We envision broad applicability of the presented approach for microfluidic perfusion co-culture of multiple cell types in the presence of fluid flow stimulation, and as a tool to investigate osteocyte mechanotransduction, as well as bone metastasis extravasation. This system could also be applied to any multicell population cross-talk studies that are typically performed using PPFCs (e.g. endothelial cells, smooth muscle cells, and fibroblasts).

1. Introduction

Bone consists of a multitude of cells, including osteoclasts (bone resorption cells), osteoblasts (bone formation cells), and osteocytes (bone cells embedded in the bone matrix) (Clarke, 2008). These cells are subjected to different mechanical stimuli and biochemical signals that modulate their response. These cellular responses can regulate a variety of bone disorders, including increasing osteoclast activity associated with osteoporosis and bone metastasis. By understanding these cellular responses, it is possible to develop novel strategies for overcoming these bone disorders and pathologies (Rochefort, 2014; Zheng et al., 2013). However, recapitulating this complex environment *in vitro* is challenging.

One common clinical intervention for these disorders is stimulating bone through exercise (Beaton et al., 2009; Nikander et al., 2010). Osteocytes are located within interstitial spaces known as lacuna, and their processes connect through narrow channels known as canaliculi, making up the lacunar-canalicular system (LCS) (Schneider et al., 2010; You et al., 2004). When a load is applied to bone, the LCS is compressed, inducing a variety of mechanical stimuli, including fluid shear stresses (FSS) (Price et al., 2011). This results in changes in the expression of osteocyte generated signals, such as receptor activator of nuclear-κ β ligand (RANKL) (Xiong and O'Brien, 2012), osteoprotegerin (OPG) (You et al., 2008a), nitric oxide (NO) (Vatsa et al., 2007), prostaglandin E2 (PGE-2) (Kitase et al., 2010), and sclerostin (Nguyen et al., 2013). Osteocytes communicate to other cells through paracrine signaling (Schaffler and Kennedy, 2012) and gap junctions (Jiang

* Corresponding author at: Department of Mechanical and Industrial Engineering, University of Toronto, 5 King's College Road, Toronto, Ontario M5S 3G8, Canada. Fax: +1 416 978 7753.
E-mail address: youlidan@mie.utoronto.ca (L. You).

http://dx.doi.org/10.1016/j.jbiomech.2017.05.012
0021-9290/

et al., 2007). Because of their thorough distribution within bone, and their sensitivity to various mechanical stimuli, osteocytes are critical in regulating the response of bone to mechanical stimulation (Bonewald and Johnson, 2008), and likely regulate many bone pathologies (Bonewald, 2004; Zhou et al., 2016).

Most *in vitro* osteocyte mechanotransduction and cell regulation studies are performed using parallel plate flow chambers (PPFC), where osteocyte-like cells are subjected to FSS, and conditioned medium is applied to different cells (Cheung et al., 2011; You et al., 2008a). However, this methodology lacks dynamic and real-time biochemical signaling between the cells involved, the cell signaling is unidirectional, and it ignores interactions of low half-life signals, such as NO (Clancy et al., 1990). Additionally, these macro-scaled chambers prevent the use of primary osteocytes (Kato et al., 1997) due to the large cell numbers required. Various microfluidic platforms have been developed to study the mechanical stimulation of bone cells. These include a multi-shear platform to investigate osteoblast calcium dynamics (Kou et al., 2011), a magnetic stimulator to promote osteoblast proliferation (Song et al., 2010), as well as a model of the LCS (You et al., 2008b). However, none of these platforms address the limitations of cellular cross-talk that currently exists with PPFCs.

To mitigate these constraints, different co-culture systems have been developed to investigate a variety of intercellular signaling pathways (Miki et al., 2012); the most common being transwell inserts. However, transwells have limited capabilities to apply FSS to cells. Specifically, rotating disks have been used to apply flow to transwells, resulting in radially dependent FSS (Taylor et al., 2007). As well, flow can only be applied to the population of cells seeded on the top of the transwell. Various microfluidic systems have also been developed to perform flow based co-culture. These devices have one cell type embedded in a gel (Chen et al., 2013; Sellgren et al., 2015), use model extracellular matrix (ECM) (Jeon et al., 2013), or use porous membranes to separate different cell populations (Booth and Kim, 2012). However, these techniques reduce signal transport between the cell populations separated by the gel (Amsden, 1998), and can be complex to fabricate for biologically focused labs.

In this work, we present a gel-free microfluidic co-culture system. High resistance side channels allow this system to apply isolated stimulatory flow (>0.5 Pa) (Li et al., 2012) while promoting signaling between different cell populations. Our device is validated through analytical modeling and experimental measurements. Finally, this device was used to investigate osteoclast precursor responses to signals produced by mechanically stimulated (fOCY) or unstimulated (nOCY) osteocytes, as well as the regulation of osteocyte mechanosensitivity by osteoclasts.

2. Materials and methods

2.1. Device development

The device models the bone microenvironment in terms of developing cell signaling gradients and fluid flow stimulation (Fig. 1A). The device consists of either 2 or 3 parallel cell culture channels (Length: 1.6 cm, Width: 1 mm, Height: 60 μm) depending on the experiment being performed. Each channel is separated by high resistance side channels (Length: 200 μm, Width: 20 μm, Height: 60 μm) at a

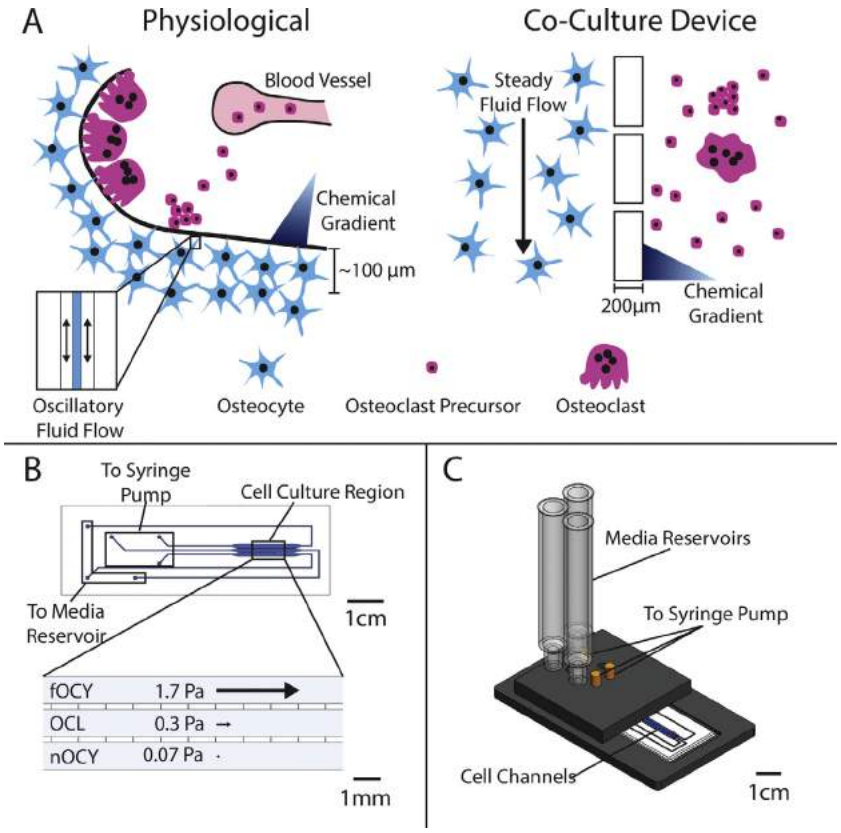

Fig. 1. (A) A direct comparison of the physiological environment of the basic multicellular unit (BMU) and our co-culture device. In both cases osteocytes are exposed to physiological levels of FSS across the cell bodies and processes. As well, osteoclast precursors (in a blood vessel *in vivo*) are exposed to an osteocyte developed signaling gradient, allowing them to migrate to the bone site, aggregate, and fuse into osteoclasts. (B) Layout of a 3-channel microfluidic device, showing placement of connections to the syringe pump and reservoir. Close up of the cell culture region shows the co-culture experimental setup, with MLO-Y4 cells seeded in the fOCY and nOCY channels and RAW264.7 cells seeded in the OCL channel. The flow setup is also presented, where the fOCY channel is subjected to a steady stimulatory flow (>0.5 Pa). (C) 3D model of the microfluidic device including stainless steel manifold, syringe reservoir and connections to syringe pump.

physiologically relevant distance (Pfeiffer, 1998) to minimize convection between channels. The device layout was chosen to fit within a previously designed manifold (Fig. 1B and C). Details of the experimental setup are described in supplement S1. Fabrication of the devices involved the development of a SU-8 (Microchem) master using standard soft lithography techniques, followed by plasma bonding a polydimethylsiloxane (Dow Corning) device onto a glass slide.

2.2. Flow isolation analysis

To validate that stimulatory flow could be isolated to one channel, a cell suspension was loaded into a 3-channel device, and the osteoclast (OCL) and nOCY channels were closed to reduce convective transfer. The fOCY channel received a steady flow of 10.3–103 μl/min, corresponding to a wall FSS, τ_{WSS}, of 0.2–2 Pa based on Eq. (1) (Bacabac et al., 2005).

$$\tau_{WSS} = \frac{6Q\mu}{h^2 w} \quad (1)$$

where Q is the fluid flow rate, μ is the dynamic viscosity of the fluid, h is the channel height, and w is the channel width. Cell streaks were recorded at 30 FPS (Video S1), and measured in ImageJ (NIH) to determine the flow velocity and resulting FSS. This was compared to an analytical model of flow (supplement S2).

2.3. Signal transport between channels

We investigated the diffusion of three signals that regulate osteoclastogenesis: RANKL, OPG, and PGE-2 (Kaji et al., 1996; Sims and Martin, 2014). To measure the transport of these signals experimentally, fluorescent dyes with similar molecular weights were perfused through one channel of a 2-channel device. 20 kDa FITC-Dextran (Sigma-Aldrich) (Ex: 490 nm, Em: 520 nm), 70 kDa FITC-Dextran (Sigma-Aldrich) (Ex: 490 nm, Em: 520 nm), and 376 Da fluorescein sodium salt (Sigma-Aldrich) (Ex: 460 nm, Em: 515 nm) modeled RANKL (Zhang et al., 2009), OPG (Wright et al., 2009), and PGE-2 respectively. One channel of a 2-channel device was loaded with the dye solution (1 mg/ml in α-minimum essential medium (α-MEM) without phenol red (Life Technologies)), and the other channel with α-MEM without phenol red. A perfusion flow of 1 μl/min was applied to both channels, and the fluorescent intensity across the non-dyed channel was quantified using ImageJ for up to 6 h. The results were compared to an analytical model of diffusion (supplement S3).

2.4. Cell culture

Osteocyte-like MLO-Y4 cells (a gift from Dr. Lynda Bonewald, Indiana University) were seeded on dishes coated with collagen (4.3% rat-tail collagen-I (Corning), 95.7% 0.02 N acetic acid (Sigma-Aldrich)). The cells were maintained with MLO-Y4 medium (94% α-MEM (Gibco), 2.5% fetal bovine serum (FBS) (Gibco), 2.5% calf serum (CS) (Gibco), 1% penicillin-streptomycin (P/S) (Gibco)). MLO-Y4 cells were grown to 70–80% confluence, and maintained up to passage 40.

RAW264.7 cells (ATCC), a model of osteoclast precursors, were maintained in uncoated dishes in RAW medium (87% Dulbecco's modified eagle medium (DMEM) (Sigma-Aldrich), 10% FBS, 2% L-Glutamine (Gibco), and 1% P/S). RAW264.7 cells were maintained up to passage 14.

2.5. Supplemental media experiment

RAW264.7 cells were seeded in RAW medium in one channel of a 2-channel device (Fig. 4A). The adjacent channel contained either RAW media as a negative control, or RAW media supplemented with 50 ng/ml of RANKL (R&D Systems). A perfusion flow of 1 μl/min was applied to both channels for six days. During the first four days, the cells were imaged at 8 fixed locations in the channel, and the cell density was quantified across the width of the channel. After six days, the number of multinucleated cells was counted across the width of the channel.

2.6. Co-culture experiment and TRAP staining

MLO-Y4 cells were seeded within the fOCY and nOCY channels on collagen, and RAW264.7 cells were in seeded in the OCL channel (Fig. 5A). The cells were perfused at 1 μl/min with MLO-Y4 and RAW264.7 media respectively. Every day, the fOCY channel received a steady FSS (2 Pa, 1 h), while the OCL and nOCY channels were blocked. During the first four days, the OCL channel was imaged at 8 fixed locations, and the RAW264.7 cell density was quantified across the width of the channel. After six days, the OCL channel was fixed and stained for tartrate resistant acid phosphatase (TRAP), a marker of osteoclast formation (You et al., 2008a), using a TRAP kit (Sigma–Aldrich). The number of osteoclasts (TRAP+, multinucleated) was counted across the width of the OCL channel.

2.7. Intracellular calcium measurement

MLO-Y4 cells were seeded in the fOCY channel of a 2-channel device on collagen. In the adjacent channel, either RAW264.7 cells (OCY-OCL) or MLO-Y4 cells (OCY-OCY) were seeded. MLO-Y4 cells were perfused with MLO-Y4 media, and RAW264.7 cells were perfused with RANKL supplemented RAW medium (10 ng/ml RANKL) at 1 μl/min. The cells were maintained for 6 days to allow the osteoclast precursors to differentiate and MLO-Y4 cells to achieve confluence. The cells were stained with Fura-2 AM dye (Life Technologies) (Ex: 340 nm/380 nm, Em: 510 nm), a ratiometric calcium indicator. Cells were fluorescently imaged for the duration of the experiment using EasyRatioPro (PTI). A 3 min baseline measurement was recorded, after which flow (2 Pa) was applied for 3 min. Finally, flow was turned off, and the cells were imaged for an additional 3 min. At least 30 cells were selected in the same field of view to be analysed. The fluorescent ratio (340 nm/380 nm) was analysed using a previously developed MATLAB script (MathWorks). A significant peak was taken to be at least twice the maximum baseline peak. The ratiometric data was converted to calcium concentration using a calibration curve developed for our imaging setup (Supplement S4).

2.8. Statistical analysis

For analysing osteoclast precursor population growth and differentiation, the OCL channel was divided into regions that were 200 μm wide (Supplement S5). Cells were quantified within these regions, and normalized to the average number of cells. Precursor densities were also normalized to the original cell seeding density. Finally, in the supplemental media experiment, RANKL precursor densities were normalised to the control results. Counts for different regions of the channel were compared using one-way analysis of variance, followed by Tukey's post hoc analysis. For the calcium experiments, the percentage of significantly responding cells and the mean magnitude of that response were compared using the student t-test with the Holm-Bonferroni correction. Statistical significance was taken at $\alpha = 0.05$.

3. Results

3.1. Fluid shear stresses in co-culture system

In the full experimental setup, a 2 Pa flow is applied to the device. Experimentally, a FSS of 1.65 Pa, 0.28 Pa, and 0.07 Pa was measured in the fOCY, OCL, and nOCY channels respectively (Fig. 2). This result is similar to our analytical prediction of a 1.54 Pa FSS in the fOCY channel. We took the threshold mechanical stimulation to be 0.5 Pa, as this was the shear stress level where Cox-2 and RANKL/OPG mRNA of MLO-Y4 cells was not significantly altered relative to static (Li et al., 2012). This suggests that the cells in the nOCY channels would not experience significant levels of mechanical stimulation.

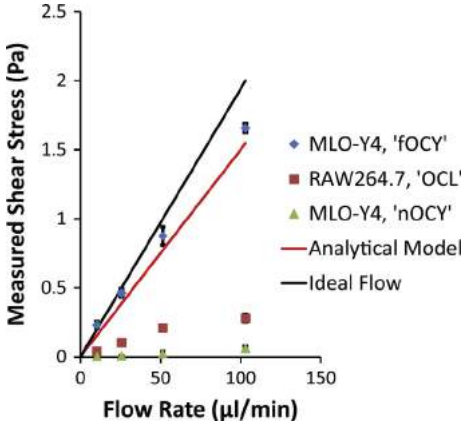

Fig. 2. FSS calculated from the flow velocities measured in each channel, given a specific input flow rate to the fOCY channel. Error bars are one standard deviation. ($N = 3+$). The black line represents 'ideal flow', where the flow remains entirely in the fOCY channel, and the red line is predicted by our analytical model. (For interpretation of the references to colour in this figure legend, the reader is referred to the web version of this article.)

3.2. Diffusion between channels during perfusion

During all experiments, a perfusion flow is applied continuously to supply nutrients to cells, and to promote the development of signal gradients between cell channels. From the obtained diffusion data (Fig. 3), we calculated the root mean square (RMS) diffusive distances to be 106 ± 17 μm for OPG, 127 ± 19 μm for RANKL, and 221 ± 31 μm for PGE-2. A 1D random walk model predicts an RMS of 81 μm for OPG, 107 μm for RANKL, and 217 μm for PGE-2, which is an under-prediction for OPG and RANKL. Similarly, our analytical model of the equilibrium signal gradient under-predicts OPG and RANKL (Fig. 3D and H). This is likely caused by small deviations in the channel heights that bias convective mass transfer to the lower resistance cell culture channels, as well as limitations of using a 1D model.

3.3. Response of osteoclast precursors to RANKL gradients

During the first 4 days, no obvious change in relative cell density was observed in the negative control (Fig. 4B and C); however, when RANKL supplemental medium was supplied, the cells preferentially increased density towards the RANKL source (Fig. 4E and F). When the supplemental media results were normalized to the negative control experiment, a significant increase in cell density within 200 μm of the RANKL channel was observed (Fig. 4I). After 6 days, there was no sign of osteoclastogenesis in the negative control (Fig. 4D), while, when a RANKL gradient was applied, multinucleated cells were observed to form, primarily within 600 μm of the RANKL source (Fig. 4G, H, and J).

3.4. Response of osteoclast precursors to signals produced by osteocytes

After 4 days the precursor density significantly increased within 200 μm of the nOCY channel (Fig. 5I). Furthermore, after 6 days a significant increase in TRAP+ multinucleated cells was also observed within 200 μm of the nOCY channel (Fig. 5J).

3.5. Osteocyte mechanosensitivity affected by osteoclasts

In both the OCY-OCY and OCY-OCL experimental groups, FSS stimulated a spike in intracellular calcium (Fig. 6A and C). Specifically, when osteocytes were co-cultured with other osteocytes, only 33 ± 7% of the cells had a significant calcium response. However, when co-cultured with osteoclasts, the percentage of responding osteocytes increased to 71 ± 14% (Fig. 6E). There was no significant difference in terms of the mean magnitude of the response for both conditions (Fig. 6F).

4. Discussion

Current PPFCs are limited when investigating mechanically regulated cell interactions. Specifically, these systems lack direct and dynamic cell signaling, allow only unidirectional signaling, and omit low half-life signal interactions. Furthermore, these macro-scaled platforms are not applicable for primary osteocyte studies due to the large number of cells required. There have been recent developments in flow based co-culture systems that use gels to isolate fluid stimulation, but these systems are limited as the use of gel restricts signal diffusion, and requires fabrication techniques

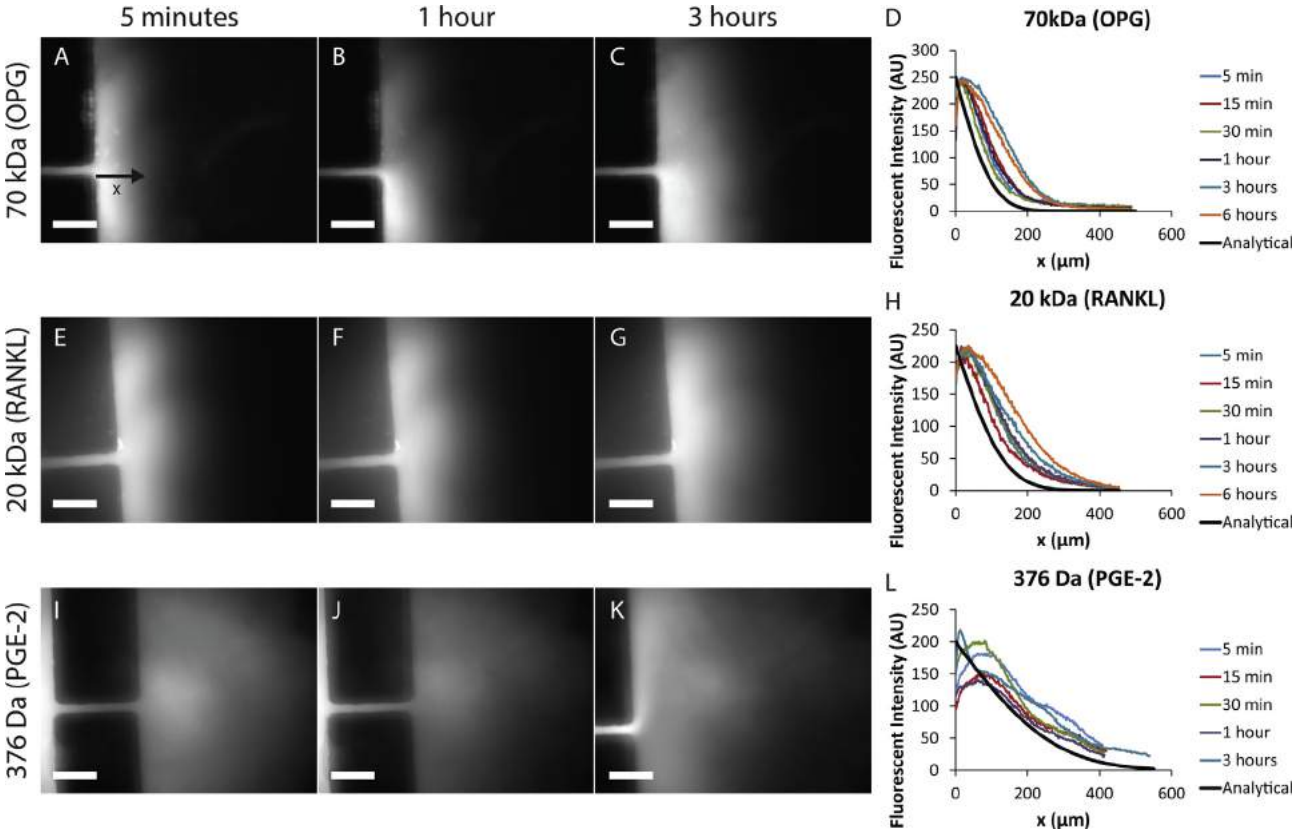

Fig. 3. Fluorescent images of signal gradients of fluorescent dye used to model (A-C) OPG, (E-G) RANKL, and (I-K) PGE-2 taken at (A, E, I) 5 min, (B, F, J) 1 h, and (C, G, K) 3 h after perfusion flow (1 μl/min) was initiated. Scale bars are 100 μm. Black axis 'x' in (A) demonstrates the position that the diffusive distance is measured from. (D, H, L) Plots of measured fluorescent intensities at different time points showing the establishment of a signaling gradient during perfusion flow compared to an analytical solution of 1D diffusion (black line).

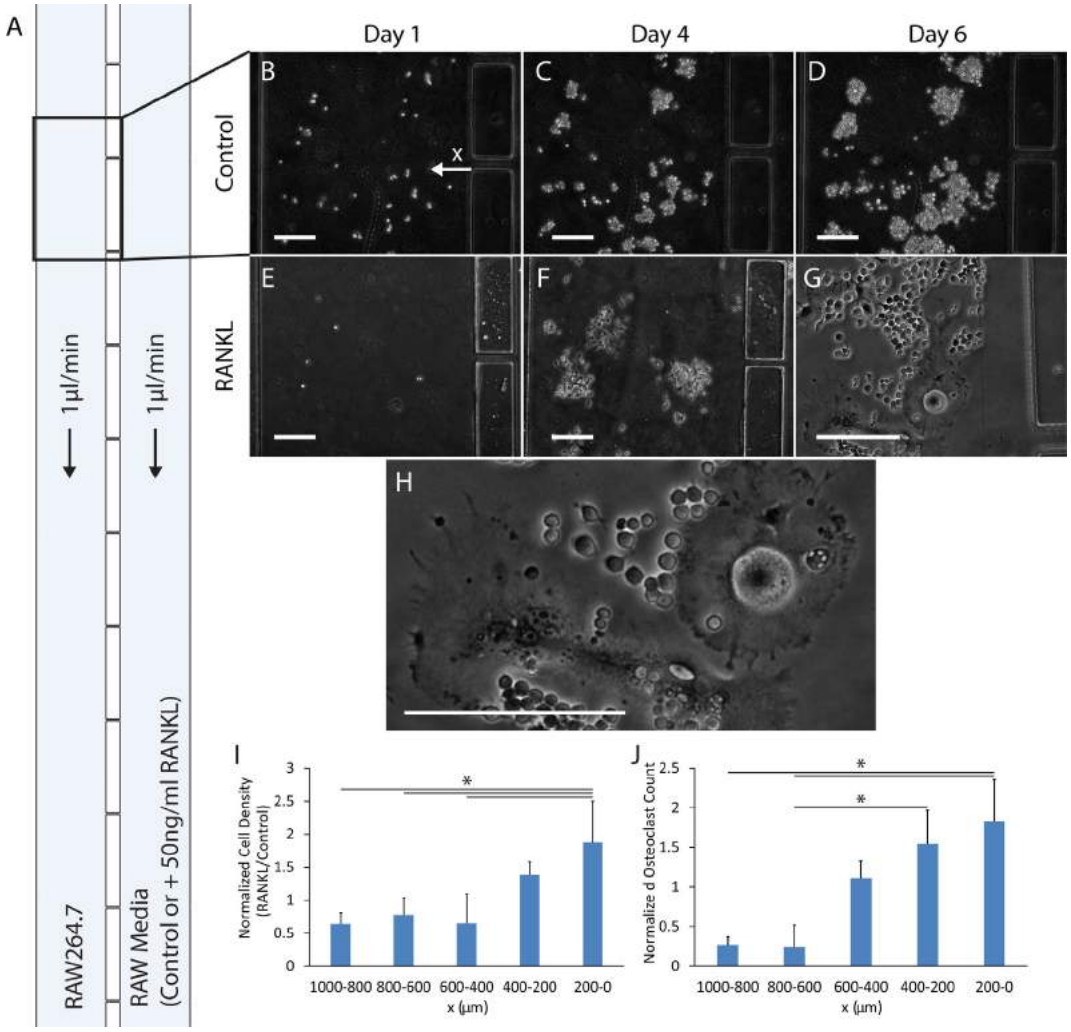

Fig. 4. (A) Device schematic showing experimental setup, with RAW264.7 cells in the left channel, and the RANKL supplemental media in the right channel (not to scale). The black rectangle represents the imaging region. (B-D) Images of negative control supplemental media experiment results after: (B) 1 day, (C) 4 days, and (D) 6 days. (E-G) Images of RANKL supplemental media experiment results after: (E) 1 day, (F) 4 days, and (G) 6 days. (H) Magnified image of osteoclasts in RANKL supplemental media experiment after 6 days. Scale bars are all 200 µm. The white axis 'x' in (B) designates distance from the supplemental media channel. (I) RANKL supplemental media cell density data normalized to the control cell density data after 4 days ($N = 3$). (J) Normalized multinucleated cell count for RANKL supplemental media experiment after 6 days ($N = 3$). All error bars are one standard deviation. $^{*}P < 0.05$.

that are challenging for labs with minimal microfabrication experience. In this study, we have developed a gel free microfluidic co-culture platform that utilises high resistance side channels to isolate stimulatory fluid flow, while promoting the development of signal gradients.

We have demonstrated that stimulatory flow (>0.5 Pa) could be confined to one channel in this device through the use of particle trace measurements (Fig. 2). This is supported by decreased levels of RANKL expression from fOCY compared to nOCY (supplement S6). In future, convective losses to the OCL and nOCY channels could be further reduced by increasing the side channel resistances. We also validated that signaling gradients could form during perfusion flow using dyes that modeled the diffusivity of signals that regulate osteoclastogenesis. The gradient of each signal varied by less than 100 µm at different time points (Fig. 3), suggesting the gradient is relatively stable. Finally, we investigated osteoclast precursor responses to this gradient. It was observed that osteoclast precursor density increased up the RANKL gradient (Fig. 4I). This relative increase in cell density could be caused by various confounding factors, such as increased proliferation, decreased cell apoptosis, or cell migration. Previous work has demonstrated that osteoclast precursor migration was promoted by RANKL (Al-Dujaili et al., 2011). However, the effect of RANKL on RAW264.7 cell proliferation and apoptosis has not been extensively investigated. We also observed increased differentiation towards the RANKL supplemented channel (Fig. 4J), where the RANKL concentration would be the greatest. RANKL is known to promote RAW264.7 cell differentiation (Xiong and O'Brien, 2012; Zhao et al., 2002) and is concentration dependent (Al-Dujaili et al., 2011). Furthermore, osteoclastogenesis rapidly decreased greater than 600 µm away from the RANKL source, which aligns well with our experimentally measured maximum RANKL diffusive distance of 450 µm (Fig. 3H).

After validation, the device was utilized to study the response of osteoclast precursors exposed simultaneously to fOCY and nOCY. We observed increased precursor density (Fig. 5I) towards the nOCY channel. We speculate that the observed increase is also caused by a combination of increased proliferation, decreased apoptosis, and migration. MLO-Y4 cells express macrophage-colony stimulating factor (M-CSF) (Zhao et al., 2002), which promotes osteoclast precursor proliferation (Biskobing et al., 1995) and inhibits apoptosis (Woo et al., 2002). As well, RANKL is

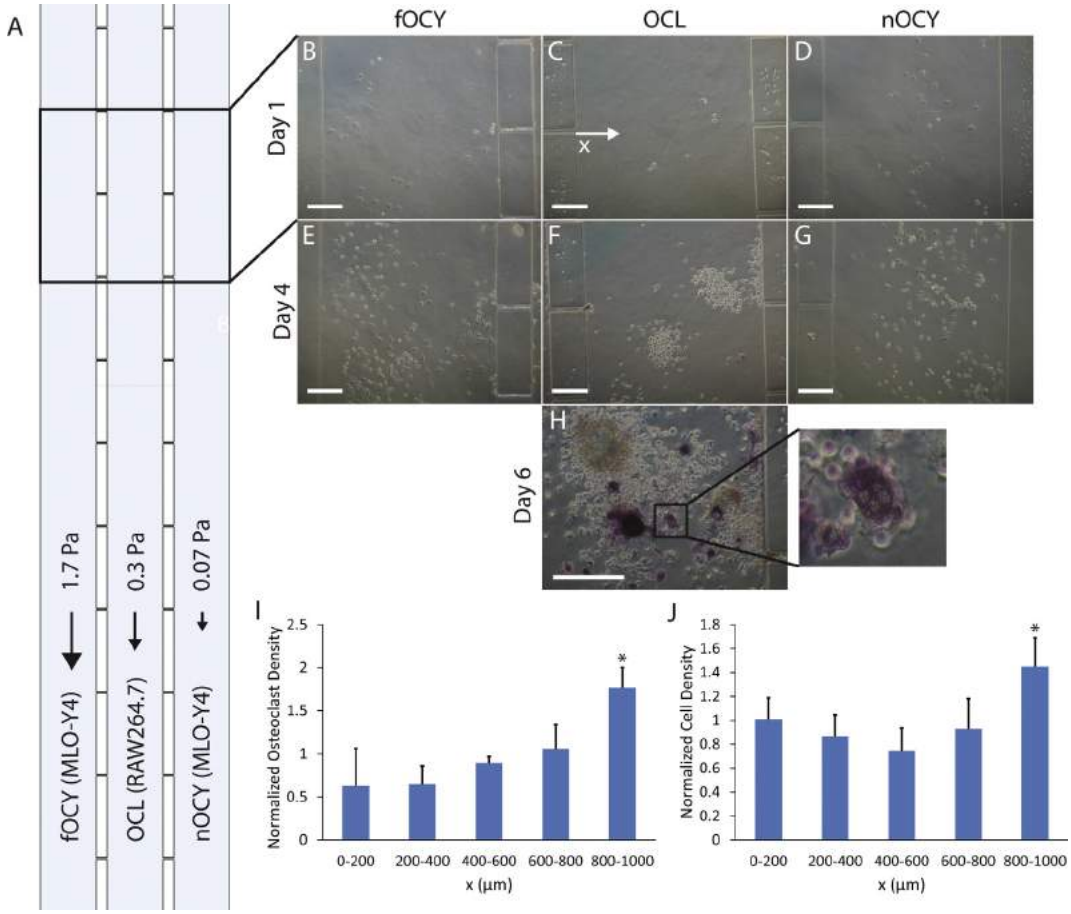

Fig. 5. (A) Device schematic demonstrating the experimental setup, with osteocytes undergoing stimulatory FSS in the fOCY channel, osteoclast precursors in the OCL channel, and unstimulated osteocytes in the nOCY channel (not to scale). The black rectangle designates the imaging region. (B-D) Images of cells in the fOCY, OCL and nOCY channel after 1 day. (E-G) Images of cells in the fOCY, OCL, and nOCY channels after 4 days. (H) Image of TRAP+ osteoclasts (red), with magnified image of an osteoclast to demonstrate multiple nuclei. Scale bars are 200 μm each. White axis 'x' in (C) demonstrates distance from the fOCY channel. (I) Plot of RAW264.7 cell density across the width of the central channel after 4 days ($N = 5$). Presented data is normalized to the original cell density and to the average cell density. (J) Quantification of multinucleated and TRAP+ cells across the width of the central channel after 6 days ($N = 4$). Error bars are one standard deviation. $^{*}P < 0.05$. (For interpretation of the references to colour in this figure legend, the reader is referred to the web version of this article.)

expressed by fOCY and nOCY, although at a decreased level in the former (You et al., 2008a), thereby promoting precursor migration. Additionally, it was observed that osteoclastogenesis increased closer to nOCY (Fig. 5J). The major regulators of osteoclast differentiation are RANKL and OPG, where RANKL binds to RANK to induce osteoclastogenesis, while OPG acts as a decoy receptor to RANKL. This ratio of RANKL to OPG is often used to quantify the potential for osteoclastogenesis, and mechanical stimulation decreases the RANKL/OPG ratio in MLO-Y4 osteocytes (You et al., 2008a). An additional potential mechanism is through osteocyte apoptosis, which is inhibited by mechanical stimulation (Bakker et al., 2004; Tan et al., 2006). It has also been demonstrated *in vitro* that apoptotic osteocytes promote osteoclast precursor migration and differentiation (Al-Dujaili et al., 2011). Additionally, osteocytes exposed to biochemical signals produced by apoptotic osteocytes also promote osteoclast differentiation (Al-Dujaili et al., 2011). *In vivo* studies have similarly shown that apoptotic osteocytes have an increased expression of RANKL, and decreased expression of OPG (Kennedy et al., 2012). This potentially suggests that osteoclast precursors are not only responding to immediate mechanically regulated signals expressed by osteocytes, but also to signals from apoptotic osteocytes. However, future studies are necessary to support these proposed mechanisms.

Finally, we investigated the role of osteoclast signaling on osteocyte mechanosensitivity. Osteocytes initially respond to FSS by increasing cytosol calcium levels (Lu et al., 2012). To observe this calcium response, MLO-Y4 cells were stained with a Fura-2 AM calcium indicator dye. When Fura-2 binds to calcium, its excitation wavelength shifts from 380 nm to 340 nm (Kong and Lee, 1995). By measuring the 340 nm/380 nm ratio in real-time, it is possible to identify a calcium response and quantify osteocyte mechanosensitivity. Specifically, we observed an increase in osteocyte mechanosensitivity when in culture with osteoclasts compared to when cultured with other osteocytes (Fig. 6E). One particular factor that is secreted by osteoclasts that can affect osteocyte mechanosensitivity is sphingosine-1-phosphate (S1P) (Pederson et al., 2008). Inhibition of sphingosine kinases in MLO-Y4 osteocytes has been shown to decrease the percentage of responding cells undergoing oscillatory fluid flow (OFF) *in vitro* (Zhang et al., 2015). That study also demonstrated that the application of S1P increased PGE-2 expression, which would promote both osteoclast (Kaji et al., 1996) and osteoblast formation (Yoshida et al., 2002), and reduced the RANKL/OPG mRNA ratio in MLO-Y4 osteocytes, thereby inhibiting osteoclast formation. Furthermore, increased mechanosensitivity in primary osteocytes could down-regulate sclerostin expression (Bonewald and Johnson, 2008), which would promote osteoblast formation (Atkins et al., 2011). However, further studies will be needed to investigate osteoclastic regulation of osteocyte mechanosensitivity and gene expression.

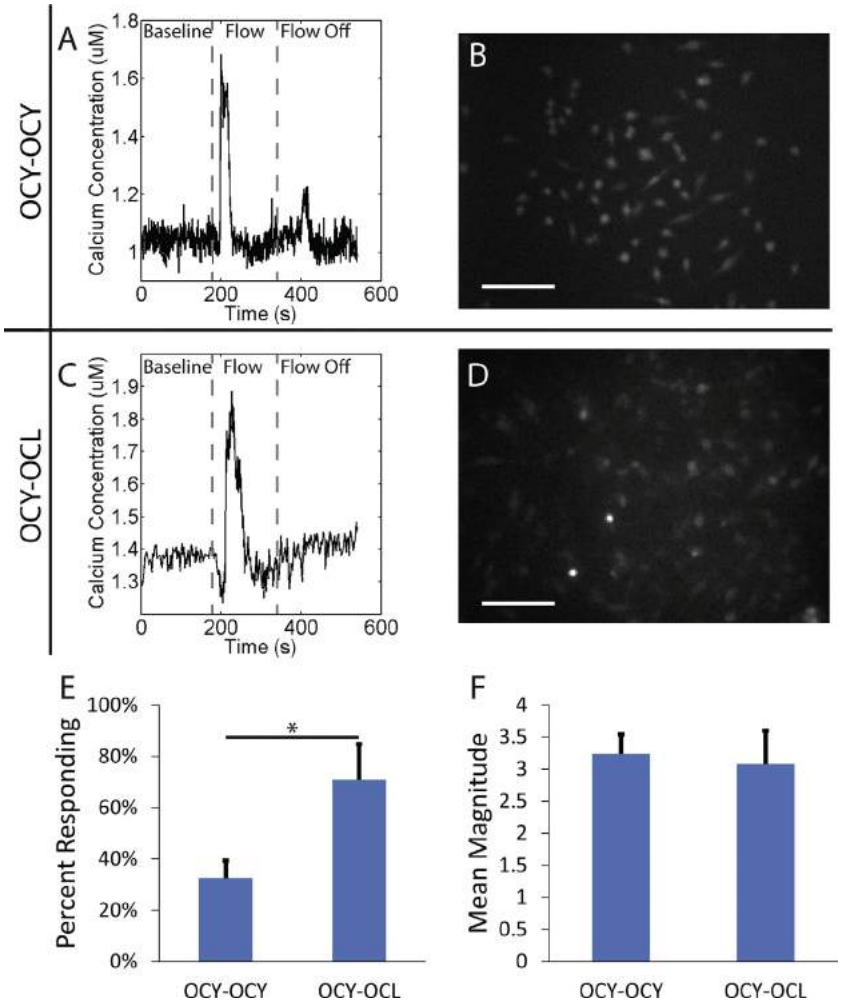

Fig. 6. Typical calcium response to flow osteocyte in co-culture with (A) osteocytes or (C) osteoclasts. Fluorescent images (ex: 340 nm) of MLO-Y4 osteocytes co-cultured with (B) osteocytes, or (D) osteoclasts. Plots of (E) percentage of cells responding to a 2 Pa flow and (F) mean magnitude of the responding cells relative to the maximum baseline peak. $N = 3$ for both, with 30+ cells being simultaneously imaged and quantified for each datum. Error bars are one standard deviation. $^{*}P < 0.05$.

To relate our preliminary observations to what is occurring physiologically, it has been suggested from computational modeling that the head of the basic multicellular unit (BMU) during bone remodeling undergoes relieved levels of stress, while stress is amplified along the walls of the BMU (van Oers et al., 2008). Our results suggest that, during bone remodeling, unstimulated osteocytes at the head of the BMU create an environment that is preferential for osteoclasts and osteoclast precursors, thereby guiding bone resorption along the loading axis of bone. Once established, osteoclasts signal to nearby osteocytes, increasing their mechanosensitivity and switching their function to promoting osteoblastogenesis. This would provide an indirect mechanism through which osteoclasts can promote bone formation.

In conclusion, this platform allows for more physiologically relevant mechanotransduction studies to be performed as it promotes real-time signalling between different cell populations at physiological length scales. However, further developments are necessary to improve the throughput and simplicity of this platform, as only two experiments could be performed simultaneously. The experimental setup could also be simplified through the utilisation of pipette loading instead of syringe pump loading, as well as through the development of novel perfusion systems. Furthermore, future studies should utilize OFF to improve the physiological relevance of the flow applied (Lu et al., 2012; Price et al., 2011). Future work using this platform will investigate how osteocytes regulate various bone pathologies, such as osteoporosis and bone metastasis, in addition to how osteoclasts regulate osteocytes. Additionally, with modifications, this platform can be applied to other cell studies that typically utilise PPFCs, such as smooth muscle cell regulation of endothelial cells to better understand the mechanisms underlying atherosclerosis (Wallace and Truskey, 2010), or investigating endothelial cell interactions with astrocytes as a model of the blood brain barrier (Takeshita et al., 2014).

Conflicts of interest

The authors declare no conflicts of interest.

Acknowledgements

We would like to thank Junyi (Danny) Cen for performing the ELISA experiments presented in the supplement. We also acknowledge postgraduate scholarships provided by the Natural Sciences and Engineering Research Council (NSERC), the NSERC CREATE Microfluidic Applications and Training in Cardiovascular Health program, the Toronto Musculoskeletal Centre, and Barbara and Frank Milligan. Funding for this research was provided by the Canadian Institutes of Health Research (fund #282723). Microfluidic fabrication facilities were provided by the Centre for

Microfluidic Systems in Chemistry and Biology at the University of Toronto that is funded by the Canada Foundation for Innovation and the Ontario Research Fund.

Appendix A. Supplementary material

Supplementary data associated with this article can be found, in the online version, at http://dx.doi.org/10.1016/j.jbiomech.2017.05.012.

References

Al-Dujaili, S.A., Lau, E., Al-Dujaili, H., Tsang, K., Guenther, A., You, L., 2011. Apoptotic osteocytes regulate osteoclast precursor recruitment and differentiation in vitro. J. Cell. Biochem. 112, 2412–2423.

Amsden, B., 1998. Solute diffusion within hydrogels. Mechanisms and models. Macromolecules 31, 8382–8395.

Atkins, G.J., Rowe, P.S., Lim, H.P., Welldon, K.J., Ormsby, R., Wijenayaka, A.R., Zelenchuk, L., Evdokiou, A., Findlay, D.M., 2011. Sclerostin is a locally acting regulator of late-osteoblast/preosteocyte differentiation and regulates mineralization through a MEPE-ASARM-dependent mechanism. J. Bone Miner. Res. 26, 1425–1436.

Bacabac, R.G., Smit, T.H., Cowin, S.C., Van Loon, J.J.W.A., Nieuwstadt, F.T.M., Heethaar, R., Klein-Nulend, J., 2005. Dynamic shear stress in parallel-plate flow chambers. J. Biomech. 38, 159–167.

Bakker, A., Klein-Nulend, J., Burger, E., 2004. Shear stress inhibits while disuse promotes osteocyte apoptosis. Biochem. Biophys. Res. Commun. 320, 1163–1168.

Beaton, R., Pagdin-Friesen, W., Robertson, C., Vigar, C., Watson, H., Harris, S.R., 2009. Effects of exercise intervention on persons with metastatic cancer: a systematic review. Physiother. Canada 61, 141–153.

Biskobing, D.M., Fan, X., Rubin, J., 1995. Characterization of MCSF-induced proliferation and subsequent osteoclast formation in murine marrow culture. J. Bone Miner. Res. 10, 1025–1032.

Bonewald, L.F., 2004. Osteocyte biology: its implications for osteoporosis. J. Musculoskelet. Neuronal Interact. 4, 101–104.

Bonewald, L.F., Johnson, M.L., 2008. Osteocytes, mechanosensing and Wnt signaling. Bone 42, 606–615.

Booth, R., Kim, H., 2012. Characterization of a microfluidic in vitro model of the blood-brain barrier (μBBB). Lab Chip 12, 1784–1792.

Chen, M.B., Srigunapalan, S., Wheeler, A.R., Simmons, C.A., 2013. A 3D microfluidic platform incorporating methacrylated gelatin hydrogels to study physiological cardiovascular cell-cell interactions. Lab Chip 13, 2591–2598.

Cheung, W.-Y., Liu, C., Tonelli-Zasarsky, R.M.L., Simmons, C.A., You, L., 2011. Osteocyte apoptosis is mechanically regulated and induces angiogenesis in vitro. J. Orthop. Res. 29, 523–530.

Clancy, R.M., Miyazaki, Y., Cannon, P.J., 1990. Use of thionitrobenzoic acid to characterize the stability of nitric oxide in aqueous solutions and in porcine aortic endothelial cell suspensions. Anal. Biochem. 191, 138–143.

Clarke, B., 2008. Normal bone anatomy and physiology. Clin. J. Am. Soc. Nephrol. 3, S131–S139.

Jeon, J.S., Zervantonakis, I.K., Chung, S., Kamm, R.D., Charest, J.L., 2013. In vitro model of tumor cell extravasation. PLoS ONE 8, e56910.

Jiang, J.X., Siller-Jackson, A.J., Burra, S., 2007. Roles of gap junctions and hemichannels in bone cell functions and in signal transmission of mechanical stress. Front. Biosci. 12, 1450–1462.

Kaji, H., Sugimoto, T., Kanatani, M., Fukase, M., Kumegawa, M., Chihara, K., 1996. Prostaglandin E2 stimulates osteoclast-like cell formation and bone-resorbing activity via osteoblasts: role of cAMP-dependent protein kinase. J. Bone Miner. Res. 11, 62–71.

Kato, Y., Windle, J.J., Koop, B.A., Mundy, G.R., Bonewald, L.F., 1997. Establishment of an osteocyte-like cell line, MLO-Y4. J. Bone Miner. Res. 12, 2014–2023.

Kennedy, O.D., Herman, B.C., Laudier, D.M., Majeska, R.J., Sun, H.B., Schaffler, M.B., 2012. Activation of resorption in fatigue-loaded bone involves both apoptosis and active pro-osteoclastogenic signaling by distinct osteocyte populations. Bone 50, 1115–1122.

Kitase, Y., Barragan, L., Qing, H., Kondoh, S., Jiang, J.X., Johnson, M.L., Bonewald, L.F., 2010. Mechanical induction of PGE2 in osteocytes blocks glucocorticoid-induced apoptosis through both the β-catenin and PKA pathways. J. Bone Miner. Res. 25, 2381–2392.

Kong, S.K., Lee, C.Y., 1995. The use of fura 2 for measurement of free calcium concentration. Biochem. Educ. 23, 97–98.

Kou, S., Pan, L., van Noort, D., Meng, G., Wu, X., Sun, H., Xu, J., Lee, I., 2011. A multishear microfluidic device for quantitative analysis of calcium dynamics in osteoblasts. Biochem. Biophys. Res. Commun. 408, 350–355.

Li, J., Rose, E., Frances, D., Sun, Y., You, L., 2012. Effect of oscillating fluid flow stimulation on osteocyte mRNA expression. J. Biomech. 45, 247–251.

Lu, X.L., Huo, B., Chiang, V., Guo, X.E., 2012. Osteocytic network is more responsive in calcium signaling than osteoblastic network under fluid flow. J. Bone Miner. Res. 27, 563–574.

Miki, Y., Ono, K., Hata, S., Suzuki, T., Kumamoto, H., Sasano, H., 2012. The advantages of co-culture over mono cell culture in simulating in vivo environment. J. Steroid Biochem. Mol. Biol. 131, 68–75.

Nguyen, J., Tang, S.Y., Nguyen, D., Alliston, T., 2013. Load regulates bone formation and Sclerostin expression through a TGFbeta-dependent mechanism. PLoS ONE 8, e53813.

Nikander, R., Sievänen, H., Heinonen, A., Daly, R.M., Uusi-Rasi, K., Kannus, P., 2010. Targeted exercise against osteoporosis: a systematic review and meta-analysis for optimising bone strength throughout life. BMC Med. 8, 1–16.

Pederson, L., Ruan, M., Westendorf, J.J., Khosla, S., Oursler, M.J., 2008. Regulation of bone formation by osteoclasts involves Wnt/BMP signaling and the chemokine sphingosine-1-phosphate. Proc. Natl. Acad. Sci. USA 105, 20764–20769.

Pfeiffer, S., 1998. Variability in osteon size in recent human populations. Am. J. Phys. Anthropol. 106, 219–227.

Price, C., Zhou, X., Li, W., Wang, L., 2011. Real-time measurement of solute transport within the lacunar-canalicular system of mechanically loaded bone: direct evidence for load-induced fluid flow. J. Bone Miner. Res. 26, 277–285.

Rochefort, G.Y., 2014. The osteocyte as a therapeutic target in the treatment of osteoporosis. Ther. Adv. Musculoskelet. Dis. 6, 79–91.

Schaffler, M.B., Kennedy, O.D., 2012. Osteocyte signaling in bone. Curr. Osteoporosis Rep. 10, 118–125.

Schneider, P., Meier, M., Wepf, R., Muller, R., 2010. Towards quantitative 3D imaging of the osteocyte lacuno-canalicular network. Bone 47, 848–858.

Sellgren, K.L., Hawkins, B.T., Grego, S., 2015. An optically transparent membrane supports shear stress studies in a three-dimensional microfluidic neurovascular unit model. Biomicrofluidics 9, 061102.

Sims, N.A., Martin, T.J., 2014. Coupling the activities of bone formation and resorption: a multitude of signals within the basic multicellular unit. BoneKEy Reports 3, 481.

Song, S.H., Choi, J., Jung, H.I., 2010. A microfluidic magnetic bead impact generator for physical stimulation of osteoblast cell. Electrophoresis 31, 2762–2770.

Takeshita, Y., Obermeier, B., Cotleur, A., Sano, Y., Kanda, T., Ransohoff, R.M., 2014. An in vitro blood–brain barrier model combining shear stress and endothelial cell/astrocyte co-culture. J. Neurosci. Methods 232, 165–172.

Tan, S.D., Kuijpers-Jagtman, A.M., Semeins, C.M., Bronckers, A.L.J.J., Maltha, J.C., Von Den Hoff, J.W., Everts, V., Klein-Nulend, J., 2006. Fluid shear stress inhibits TNFα-induced osteocyte apoptosis. J. Dent. Res. 85, 905–909.

Taylor, A.F., Saunders, M.M., Shingle, D.L., Cimbala, J.M., Zhou, Z., Donahue, H.J., 2007. Mechanically stimulated osteocytes regulate osteoblastic activity via gap junctions. Am. J. Physiol. - Cell Physiol. 292, C545–C552.

van Oers, R.F., Ruimerman, R., Tanck, E., Hilbers, P.A., Huiskes, R., 2008. A unified theory for osteonal and hemi-osteonal remodeling. Bone 42, 250–259.

Vatsa, A., Smit, T.H., Klein-Nulend, J., 2007. Extracellular NO signalling from a mechanically stimulated osteocyte. J. Biomech. 40, S89–S95.

Wallace, C.S., Truskey, G.A., 2010. Direct-contact co-culture between smooth muscle and endothelial cells inhibits TNF-α-mediated endothelial cell activation. Am. J. Physiol. - Heart Circ. Physiol. 299, H338–H346.

Woo, K.M., Kim, H.M., Ko, J.S., 2002. Macrophage colony-stimulating factor promotes the survival of osteoclast precursors by up-regulating Bcl-XL. Exp. Mol. Med. 34, 340–346.

Wright, H.L., McCarthy, H.S., Middleton, J., Marshall, M.J., 2009. RANK, RANKL and osteoprotegerin in bone biology and disease. Curr. Rev. Musculoskelet. Med. 2, 56–64.

Xiong, J., O'Brien, C.A., 2012. Osteocyte RANKL: new insights into the control of bone remodeling. J. Bone Miner. Res. 27, 499–505.

Yoshida, K., Oida, H., Kobayashi, T., Maruyama, T., Tanaka, M., Katayama, T., Yamaguchi, K., Segi, E., Tsuboyama, T., Matsushita, M., Ito, K., Ito, Y., Sugimoto, Y., Ushikubi, F., Ohuchida, S., Kondo, K., Nakamura, T., Narumiya, S., 2002. Stimulation of bone formation and prevention of bone loss by prostaglandin E EP4 receptor activation. Proc. Natl. Acad. Sci. USA 99, 4580–4585.

You, L., Temiyasathit, S., Lee, P., Kim, C.H., Tummala, P., Yao, W., Kingery, W., Malone, A.M., Kwon, R.Y., Jacobs, C.R., 2008a. Osteocytes as mechanosensors in the inhibition of bone resorption due to mechanical loading. Bone 42, 172–179.

You, L., Temiyasathit, S., Tao, E., Prinz, F., Jacobs, C.R., 2008b. 3D microfluidic approach to mechanical stimulation of osteocyte processes. Cell. Mol. Bioeng. 1, 103–107.

You, L., Weinbaum, S., Cowin, S.C., Schaffler, M.B., 2004. Ultrastructure of the osteocyte process and its pericellular matrix. Anat. Rec. - Part A Discoveries Mol., Cell., Evol. Biol. 278, 505–513.

Zhang, J.-N., Zhao, Y., Liu, C., Han, E.S., Yu, X., Lidington, D., Bolz, S.-S., You, L., 2015. The role of the sphingosine-1-phosphate signaling pathway in osteocyte mechanotransduction. Bone 79, 71–78.

Zhang, S., Liu, C., Huang, P., Zhou, S., Ren, J., Kitamura, Y., Tang, P., Bi, Z., Gao, B., 2009. The affinity of human RANK binding to its ligand RANKL. Arch. Biochem. Biophys. 487, 49–53.

Zhao, S., Kato, Y., Zhang, Y., Harris, S., Ahuja, S.S., Bonewald, L.F., 2002. MLO-Y4 osteocyte-like cells support osteoclast formation and activation. J. Bone Miner. Res. 17, 2068–2079.

Zheng, Y., Zhou, H., Dunstan, C.R., Sutherland, R.L., Seibel, M.J., 2013. The role of the bone microenvironment in skeletal metastasis. J. Bone Oncol. 2, 47–57.

Zhou, J.Z., Riquelme, M.A., Gu, S., Kar, R., Gao, X., Sun, L., Jiang, J.X., 2016. Osteocytic connexin hemichannels suppress breast cancer growth and bone metastasis. Oncogene 35, 5597–5607.